COMMUNICATION

Photoactive g-C_3N_4 Nanosheets for Light-Induced Suppression of Alzheimer's β-Amyloid Aggregation and Toxicity

*You Jung Chung, Byung Il Lee, Jong Wan Ko, and Chan Beum Park**

Alzheimer's disease (AD) is a fatal neurodegenerative disease that accompanies symptoms of dementia such as memory loss and cognitive disability. AD has increased rapidly in the past decades, now affecting more than 11% of the population aged over 65.[1] The noticeable hallmark pathology of AD is progressive accumulation of the protein fragment called β-amyloid (Aβ) in the brain, which induces damage and death of neurons. The cleavage of β-amyloid precursor protein (β-APP) by β- or γ-secretases releases abnormal Aβ monomers that have 39–42 amino acids,[2] which gradually self-assemble to form β-sheet–rich, intermediate oligomers and mature fibrils through nucleation and polymerization.[3] Biological functions of Aβ aggregates are not well defined so far; intermediate oligomers are reported to be more toxic than end-stage amyloid fibrils.[4] Thus, effective suppression of Aβ aggregation and toxicity is considered a key strategy for treating AD.

Herein we report that graphitic carbon nitride (g-C_3N_4) nanosheets act as an effective inhibitor of Aβ aggregation and toxicity under light irradiation. Photodynamic therapy (PDT) is an attractive, noninvasive strategy that had been applied to cancer treatment.[5] It employs light and a photosensitizer to treat a localized spot by using generated reactive oxygen species (ROS). Interests on PDT have rapidly growing because of its minimal invasiveness and many different types of nanomaterials have been applied as in vivo or in vitro agents for PDT.[6] However, PDT for AD treatment is still in its infancy, not a mature therapeutic method at present. In the previous works,[7–9] molecular dyes such as rose bengal and porphyrin were studied for their efficacy on photoinduced inhibition of Aβ aggregation. The inhibitory effect was attributed to the generation of ROS by the molecular photosensitizers, which induced structural change of Aβ. According to our study, photosensitized g-C_3N_4 generates ROS through an electrical pathway between its valence and conduction bands under an excitation state, which further prevents the aggregation of Aβ monomers by photo-oxidation, as depicted in **Scheme 1**. g-C_3N_4 is a metal-free material of only carbon and nitrogen-based structure called tri-s-triazine, which is nontoxic, abundant, and cost-effective.[10,11] While there are only a few studies about biomedical applications of g-C_3N_4, good biocompatibility of g-C_3N_4 has been confirmed recently through its use in cancer diagnosis, drug delivery, and cell imaging.[12–14] g-C_3N_4 has been applied to solar water-splitting and hydrogen generation as a promising photocatalyst because of its high thermal and chemical stabilities.[15] It has a narrow bandgap (2.6–2.8 eV) that can excite electrons under visible light unlike other photoactive materials (e.g., TiO_2, ZnO, polyoxometalate). Furthermore, electrical and optical properties of g-C_3N_4 can be tuned by controlling synthetic conditions (e.g., condensation temperature) or by metal doping.[16,17]

We synthesized g-C_3N_4 using dicyandiamide as a precursor with ammonium chloride as a sacrificial gas exfoliator to produce a sheet-like morphology having a high surface area.[18] According to our observation using an atomic force microscopy, as-prepared g-C_3N_4 was properly exfoliated and dispersed in deionized water (Figure S1a, Supporting Information). The exfoliated g-C_3N_4 sheets exhibited uniformly thin-layered structure, having a thickness of 0.9–1.1 nm and a width of 0.4–1.5 μm. The transmission electron microscopy image in Figure S1b of the Supporting Information shows a typical crumpled but sheet-like morphological characteristic of g-C_3N_4. We further analyzed the exfoliated g-C_3N_4 sheets by X-ray diffraction (XRD) and Fourier transform-infrared spectroscopy (FTIR). The XRD patterns in Figure S2a of the Supporting Information reveal weaker peaks at around 27.4°(002) and 13°(001), which are attributed to the interlayer stacking and in-plane repeating motif, respectively, of triazine unit. This result indicates less stacked and more sheet-like characteristic of the as-prepared g-C_3N_4 than bulk g-C_3N_4. The FTIR spectra in Figure S2b of the Supporting Information shows peaks at around 3000–3500, 1200–1800, and 808 cm^{-1} of wave number, which signify N–H stretching, C–N heterocyclic vibration, and s-triazine ring structure, respectively.[19] We further analyzed optical properties of exfoliated g-C_3N_4 by UV–vis absorbance and photoluminescence spectroscopies. Exfoliated g-C_3N_4 exhibited 2.6 eV of narrower bandgap and weaker fluorescence intensity than bulk one (Figure S3, Supporting Information).We investigated the effect of photoactive g-C_3N_4 on Aβ aggregation by adding g-C_3N_4 to Aβ monomer-containing buffer and incubating the solution at 30 °C for 24 h under illumination of a white light-emitting diode (LED). The atomic force microscopy (AFM) images in **Figure 1**a show that light itself did not have any effect, as plenty of amyloid aggregates and fibrils were observed. Likewise, there was no significant effect on Aβ aggregation with g-C_3N_4 under dark conditions. In contrast, only a limited number of Aβ fragments were found in the presence of g-C_3N_4 under light illumination. According to native gel electrophoresis analysis of Aβ aggregates

Y. J. Chung, B. I. Lee, J. W. Ko, Prof. C. B. Park
Department of Materials Science and Engineering
Korea Advanced Institute of Science
and Technology (KAIST)
335 Science Road, Yuseong-gu
Daejeon 305-701, South Korea
E-mail: parkcb@kaist.ac.kr

DOI: 10.1002/adhm.201500964

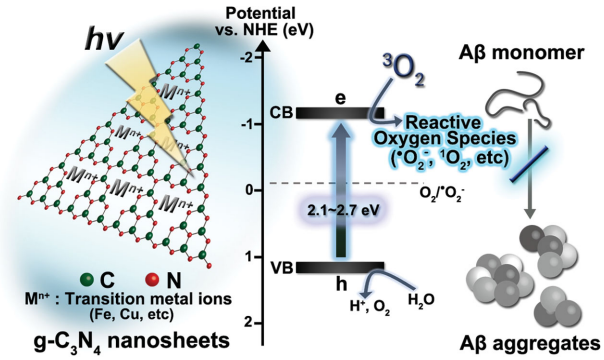

Scheme 1. A schematic illustration of g-C_3N_4 nanosheets as a β-amyloid (Aβ) aggregation inhibitor. When the g-C_3N_4 nanosheets are exposed to visible light, reactive oxygen species (ROS) are generated by the interaction between photoexcited g-C_3N_4 and oxygen molecules. Highly reactive ROS then trigger peptide oxidation that suppresses further fibril-formation of Aβ.

(Figure 1b), Aβ incubated with g-C_3N_4 under LED illumination showed a strong band of 4 kDa monomers while bands of small oligomers (15–20 kDa) were mostly found in other cases. It indicates that photoactivated g-C_3N_4 has a significant inhibitory effect on Aβ aggregation. We further validated the efficacy of g-C_3N_4 by circular dichroism (CD) analysis (Figure 1c). In the absence of g-C_3N_4, the CD spectrum presented a positive band at 195 nm and a negative band at 215 nm, which corresponds to the typical peaks of β-sheet-rich secondary structure of peptides.[20] Similar peak shape was observed under dark conditions, even in the presence of g-C_3N_4. On the contrary, when Aβ monomers were incubated with g-C_3N_4 under light illumination, there was a remarkable change in the CD spectrum; a negative band at around 198–200 nm appeared, which stands for predominant random structures of Aβ, less aggregated or fibrilized by conformational transition of Aβ peptides. To analyze the effect on Aβ aggregation according to the concentration of photoactivated g-C_3N_4, we conducted thioflavin-T (ThT) assay.[21] As shown in Figure 1d, the intensity of ThT fluorescence became lower with the increasing concentration of photoactivated g-C_3N_4, unlike the negligible effect in the absence of light illumination. In the CD spectrum (Figure S4, Supporting Information), it was analogous to the ThT result that gradual decrease in bands at 195 and 215 nm were observed with increasing of g-C_3N_4 concentration. According to various

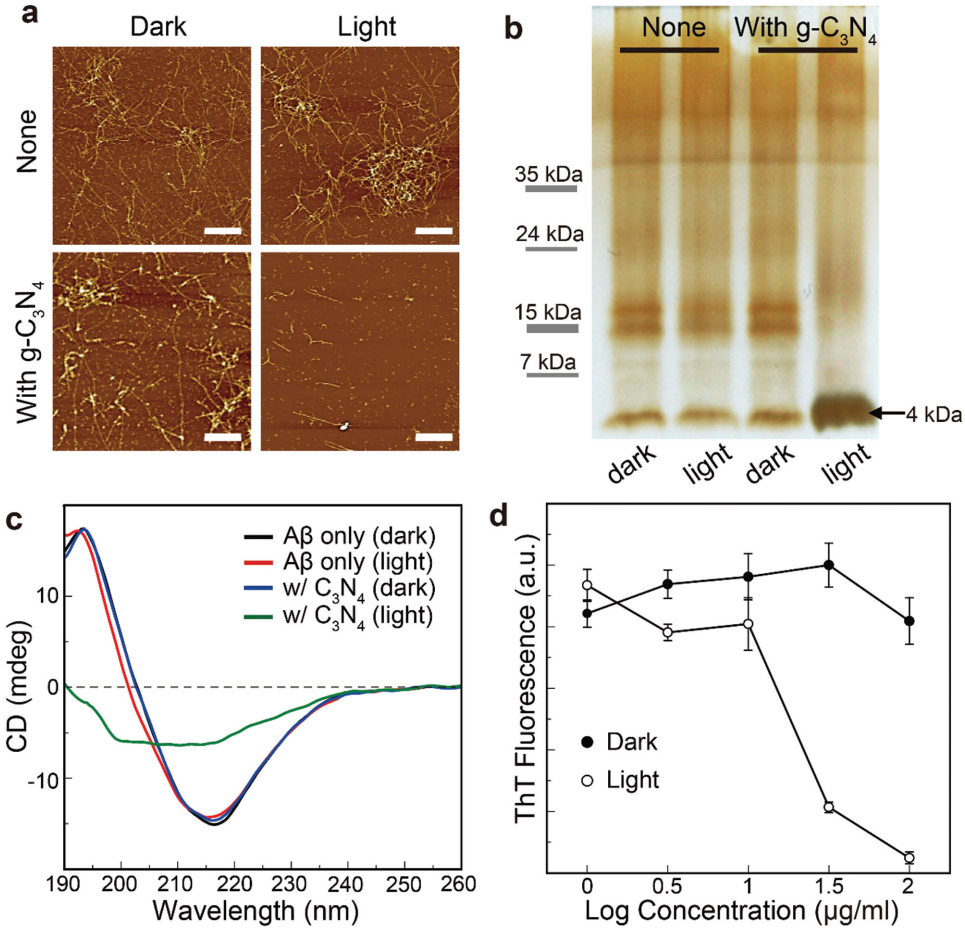

Figure 1. a) Ex situ AFM images of Aβ aggregates. Scale bars: 1 μm. b) Silver-stained native gel electrophoresis of Aβ aggregates with/without g-C_3N_4, that were illumunated (light) or not (dark). c) CD spectroscopy of Aβ aggregates in the conditions indicated. d) Normalized ThT fluorescence of Aβ aggregates for different concentrations of coincubated g-C_3N_4, n = 3. Aβ was incubated with/without g-C_3N_4 (100 μg mL^{-1} in the case of a–c) under dark or white LED for 24 h at 30 °C.

incident lights using red, green, and blue LEDs, differential effect was induced to Aβ aggregation. Due to emission discrepancy of each LED (Figure S5, Supporting Information), the highest photon energy was applied to g-C_3N_4 under blue LED and showed stronger inhibition than in the case of red or green LED. This result implies that g-C_3N_4 concentration or overlap between LED emission and g-C_3N_4 absorbance determines the degree of inhibition efficacy on Aβ aggregation.

The light-induced inhibition on Aβ aggregation is attributed to the generation of oxidative ROS intermediates through the reduction of molecular oxygen by electron transfer as well as energy transfer from photoexcited g-C_3N_4. According to the literature,[22,23] the conduction band potential of g-C_3N_4 is high enough to convert O_2 in ground-state to ROS, such as $^{\bullet}O_2^-$, via direct electron transfer under visible light. To analyze the role of O_2, we observed the photoinduced inhibitory effect of g-C_3N_4 on Aβ aggregation under Ar-purged, oxygen-depleted conditions. As shown in **Figure 2**a, the CD spectrum changed significantly under anaerobic condition showing a profile of dominant β-sheet-rich secondary structures of Aβ, which indicates the critical role of O_2 in Aβ aggregation inhibition by photoactivated g-C_3N_4. We further examined the phenomenon by using triethanolamine (TEOA), a hole scavenger, which reduces electron-hole recombination of photoactive materials. According to our analysis by ThT assay (Figure 2b), the degree of Aβ aggregation decreased with the addition of TEOA in the g-C_3N_4 solution. It suggests that TEOA promotes electrons in the conduction band of g-C_3N_4 to generate more ROS such as $^{\bullet}O_2^-$ (Figure S6, Supporting Information). By using superoxide dismutase (SOD), a selective quencher of $^{\bullet}O_2^-$,[24] we investigated the effect of $^{\bullet}O_2^-$ on Aβ aggregation. Both CD spectra and ThT assay results (Figure S7, Supporting Information) show that the inhibitory efficacy on Aβ aggregation was reduced in the presence of SOD under light illumination. This result implies that $^{\bullet}O_2^-$ is a primary oxidant toward the prevention of Aβ aggregation. Singlet oxygen ($^1O_2$) is known to be a major ROS produced from $^{\bullet}O_2^-$.[25] We analyzed the generation of $^1O_2$ by using SOSG (Singlet Oxygen Sensor Green reagent) under dark and light conditions. As presented in Figure 2c, while nearly none of $^1O_2$ was observed in the case of dark condition, amount of $^1O_2$ was significantly increased in the presence of g-C_3N_4 and light illumination. We verified the oxidation of Aβ by ROS through a 2,4-dinitrophenylhydrazine (DNPH) assay. The DNPH reacts with carbonyl groups of an oxidized protein and produces 2,4-dinitrophenylhydrazone that exhibits a characteristic absorption peak at 370 nm.[26] According to our result

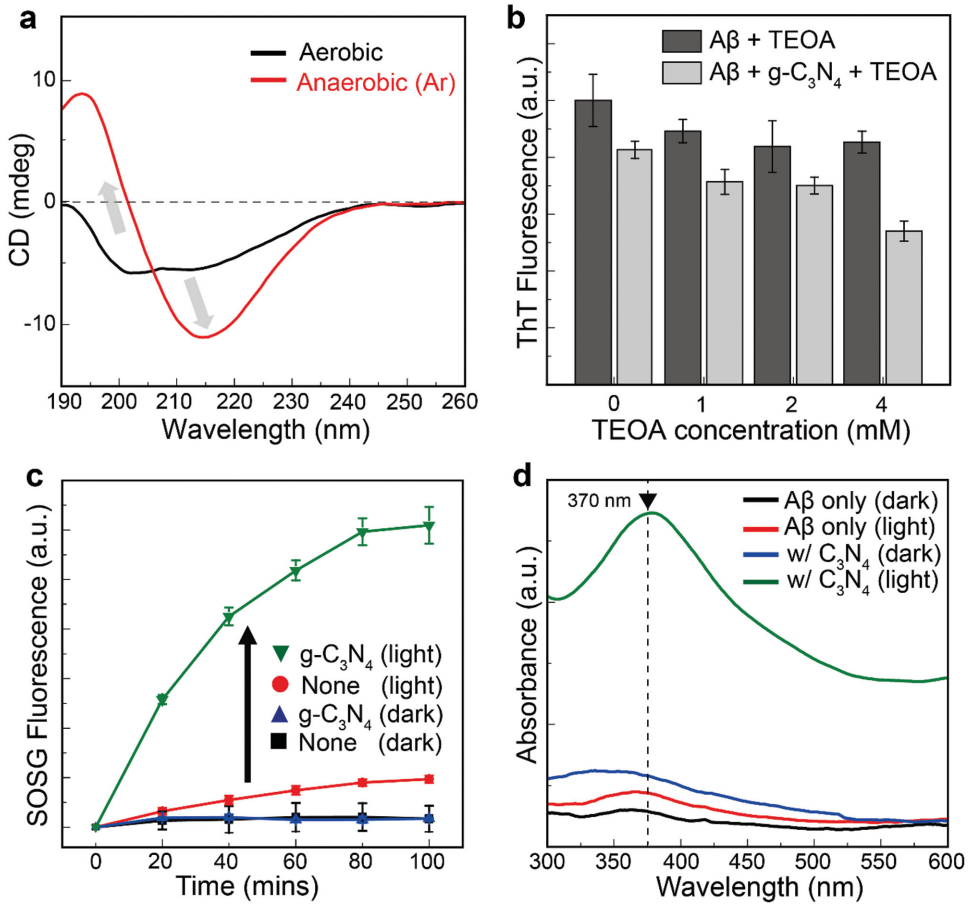

Figure 2. a) CD spectra comparing the inhibitory effect under aerobic and Ar-purged anaerobic conditions in the presence of g-C_3N_4. b) Normalized ThT fluorescence for different TEOA concentrations in Aβ aggregates with g-C_3N_4 solution (50 μg mL^{-1}), n = 3. c) Normalized singlet oxygen generation fluorescence of g-C_3N_4 under dark or white LED irradiation for 100 min, n = 3. d) DNPH assay of Aβ aggregates incubated with/without g-C_3N_4 under dark or white LED irradiation for 24 h at 30 °C. Concentration of g-C_3N_4 was 100 μg mL^{-1} in the case of (a), (c), and (d).

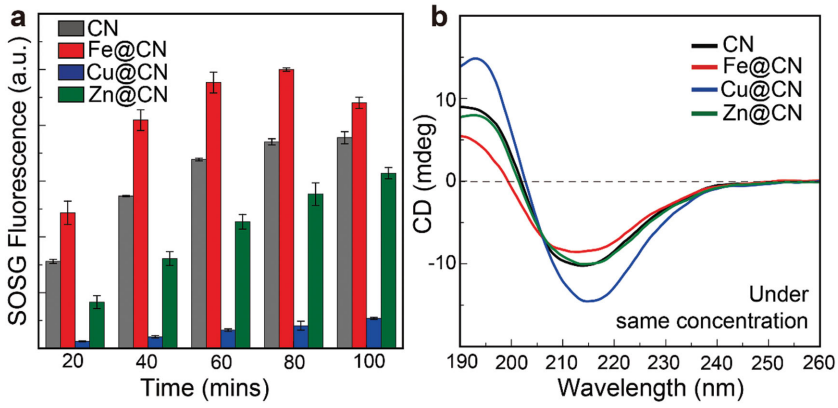

Figure 3. a) Normalized singlet oxygen generation fluorescence of CN and metal-ion-doped g-C_3N_4 (metal@CN, 100 μg mL^{-1}) under white LED irradiation for 100 min, n = 3. b) CD spectroscopy of CN and metal@CN. Aβ aggregates were incubated with CN and metal@CN ($10^{1.5}$ μg mL^{-1}) under white LED irradiation for 24 h at 30 °C.

(Figure 2d), the 370 nm peak appeared only in the presence of g-C_3N_4 and light, indicating photoinduced oxidation of Aβ.

Transition metal elements (e.g., Fe, Cu, Zn) had been applied to g-C_3N_4 for the enhancement of electrical, optical, or catalytic properties.[27] In our study, we investigated whether Aβ aggregation can be modulated by bandgap-tuning of g-C_3N_4. Modified g-C_3N_4 with metal ions (metal@CN), which were synthesized by doping of Fe, Cu, and Zn ions into g-C_3N_4 by thermal condensation reactions, showed significantly higher and broader UV–vis absorbance under visible light range (Figure S8a, Supporting Information). Bandgaps of metal@CN were estimated to be 2.1–2.6 eV, narrower than that (2.6–2.7 eV) of bare g-C_3N_4. In spite of the enhancement of optical properties, notable change in structural and chemical properties by metal doping in g-C_3N_4 was not observed (Figure S8b, Supporting Information). According to FTIR spectra, the peaks of metal@CN at around 3000–3500 and 808 cm^{-1} of wave number were similar to those of g-C_3N_4 (CN), although peak intensities slightly decreased. It indicates lesser bonding of C–N, C=N, and N–H, which is attributed to metal insertion into the framework of g-C_3N_4.[28] According to the SOSG data of metal@CN (**Figure 3**a), singlet oxygen generation by each metal@CN was in the order of Fe@CN > CN > Zn@CN > Cu@CN. Metal doping of g-C_3N_4 was reported to induce a shift in band potential.[29] Conduction band potential of Fe@CN is slightly more negative than O_2 redox potential so that Fe ions boost charge carrier transfer and O_2 reduction reaction, but that of Zn@CN or Cu@CN is insufficient for ROS generation. The differential amount of generated ROS resulted in different inhibitory effect of metal@CN against Aβ aggregation according to CD analysis (Figure 3b); Fe@CN showed the highest degree of inhibition, but Cu@CN exhibited negligible effect. We attribute the different inhibitory efficacy of metal@CN to the shift of band potential and bandgap change that affects electron transfer to O_2.

We investigated cytotoxicity of Aβ aggregates and g-C_3N_4 on PC12 cells by using 3-(4,5-dimethylthiazol-2yl)-2,5-diphenyltetrazolium bromide (MTT) assay.[30] Compared to pristine cells (control), cells that were coincubated with as-formed Aβ aggregates for 12 h at 37 °C showed significantly reduced viability (≈55%) (**Figure 4**a), indicating that Aβ aggregates injure cells. In the case of cells cultured with Aβ aggregates that were formed with g-C_3N_4 (or Fe@CN) under dark conditions, cell viability was similarly low. In contrast, cells incubated with Aβ aggregates that were oxidized by g-C_3N_4 (or Fe@CN) under LED illumination presented approximately 87% and 91% of viabilities, respectively, which are comparable to the control data. Note that g-C_3N_4 and metal@CN did not induce noticeable cell death in the wide range of concentration (0–100 μg mL^{-1}) under dark and light conditions (Figure 4b and Figure S9, Supporting Information). The result indicates that g-C_3N_4 and metal@CN are biocompatible, and cell damage by the photogenerated ROS from the materials is negligible. Overall, our results suggest that photoactivated g-C_3N_4 (with or without metal doping) suppresses Aβ aggregation and cytotoxicity.

In summary, we validated that the formation of toxic Aβ aggregates is effectively inhibited by photoinduced g-C_3N_4. Under visible-light illumination, exfoliated g-C_3N_4 nanosheets generated oxidative ROS, such as superoxide anion, singlet oxygen, via photoinduced electron transfer, which oxidized Aβ peptides and blocked further fibrillation. Induction efficiency of of Aβ aggregation inhibition increased with the concentration of g-C_3N_4 and with the overlap of absorbance with LED emission. Moreover, doped transition metal ions (e.g., iron) in g-C_3N_4 nanosheets accelerated the activity of charge transfer between valence and conduction bands of g-C_3N_4, which resulted in higher ROS generation and inhibitory effect on Aβ aggregation. Visible light-active g-C_3N_4 is a biocompatible suppressor of Aβ aggregation and toxicity, and can be a promising

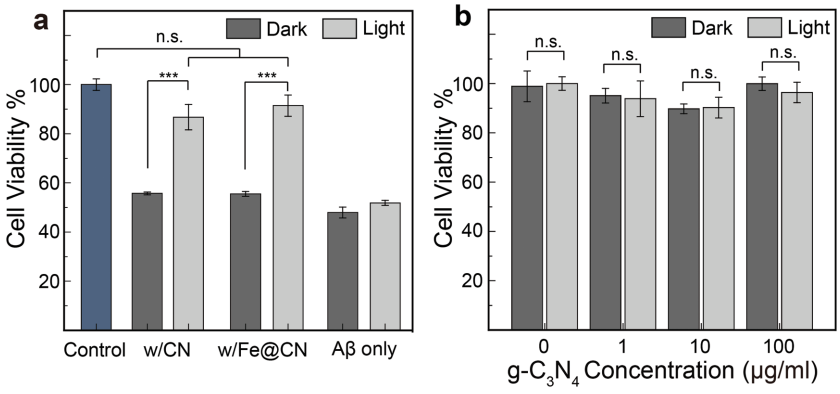

Figure 4. Cytotoxicity assays of cells incubated under different conditions (n = 3, ***p < 0.001). a) Incubation with Aβ aggregates that pre-formed with or without 100 μg mL^{-1} of g-C_3N_4 or Fe-doped g-C_3N_4 under dark or white LED illumination. b) Incubation of cells with pristine g-C_3N_4 (0, 1, 10, and 100 μg mL^{-1}) under dark or white LED illumination for 30 min. Statistical analysis was carried out by means of one-way analysis of variance (ANOVA).

material for Aβ-targeted AD treatments in the future. Further in vivo studies are needed to evaluate the potential of g-C_3N_4 for clinical applications.

Experimental Section

Materials: Human Aβ_{42} peptide was obtained from rPeptide (Bogart, GA) as a lyophilized powder. Dicyandiamide, ammonium chloride, triethanolamine, superoxide dismutase, ferrocene, $CuCl_2{\cdot}2H_2O$, $ZnCl_2$, hexafluoro-2-propanol, thioflavin T, 2,4-dinitrophenylhydrazine (DNPH), and 3-(4,5-dimethylthiazol-2yl)-2,5-diphenyltetrazolium bromide (MTT) were purchased from Sigma-Aldrich Chemical Co., (St Louis, MO). For in vitro cytotoxicity experiments, RPMI 1640, horse serum (HS), fetal bovine serum (FBS), and antibiotics were purchased from Welgene Inc., Korea.

Synthesis of g-C_3N_4 Nanosheets and Metal-doped g-C_3N_4: g-C_3N_4 nanosheets were prepared by using dicyandiamide as a precursor and ammonium chloride (NH_4Cl) as a supplement according to the literature.[18] Briefly, dicyandiamide was fully mixed with ammonium chloride by 1:5 of weight ratio and then put into an alumina crucible. Powders were synthesized by heating at 550 °C for 4 h at a rate of 3 °C min^{-1}. Then, g-C_3N_4 was dispersed in deionized water and sonicated for a few hours for further exfoliation. Metal ion-doped g-C_3N_4 nanosheets were synthesized by mixing 3 g of dicyandiamide with 2 mmol of each metal ion precursor (ferrocene, $CuCl_2{\cdot}2H_2O$, and $ZnCl_2$) before heating.[17] Thermal condensation was conducted under the same condition, as described above. After thermal processing, powders were washed several times with deionized water to eliminate unbound ions and were sonicated for further exfoliation.

Characterization of g-C_3N_4: We analyzed the morphology of as-prepared g-C_3N_4 by using a multimode AFM (Digital Instruments Inc., USA) with a NCHR silicon cantilever (Nanosensors Inc., Switzerland) and a transmission electron microscopy (TEM, FEI Company, USA). Crystalline and chemical properties were estimated by X-ray diffractometer (D/MAX-RB X-ray Diffractometer, Rigaku Co., Japan) with a scan rate of 4° min^{-1}, Cu Kα radiation of wavelength 1.5418 Å, and Fourier transform infrared spectrophotometer (FT-IR 200, Jasco Inc., Japan). Optical properties including absorbance and photoluminescence of g-C_3N_4 were investigated by UV–vis absorption spectrophotometer (Jasco Inc., Japan) and spectrofluorophotometer (Shimadzu Inc., Japan).

Preparation of Monomeric Aβ Solution: Human Aβ_{42} (1 mg) was dissolved in hexafluoro-2-propanol (HFIP) and kept overnight at room temperature. The solution was divided into microcentrifuge tubes (1/16 mg aliquots), and put into a vacuum desiccator for evaporation until film-like lyophilized Aβ_{42} was obtained. Dried Aβ_{42} films were stored at −20 °C. Monomeric Aβ_{42} was dissolved in 30 µL of mixture that included CH_3CN (300×10^{-6} M), Na_2CO_3 (300×10^{-6} M), and NaOH (250×10^{-3} M), then sonicated for 30 min. The solution was further diluted with a phosphate buffer (8.5×10^{-3} M) containing NaCl (8.5×10^{-3} M), Na_2CO_3 (14×10^{-6} M), NaOH (0.85×10^{-3} M), and acetonitrile (6.0%; final pH 8.0) to a final concentration of 40×10^{-6} M.

Inhibition of Aβ Aggregation under Visible Light Irradiation: A commercial white LED lamp (Prism., Korea) was used as a light source. The glass vials containing 40×10^{-6} M of Aβ_{42} solution were exposed to visible light and then incubated for 24 h at 30 °C.

AFM Analysis: Incubated Aβ_{42} solutions were deposited and allowed to adsorb onto cleaved mica for 20 min. AFM images were captured by the instrument (Digital Instruments Inc., USA) in a trapping mode under air using a NCHR silicon cantilever (Nanosensors Inc., Switzerland).

Native Gel Electrophoresis and Silver Staining: Incubated Aβ_{42} solutions were diluted with a loading buffer containing 50×10^{-3} M Tris HCl, pH 6.8, 10% glycerol, 2% SDS, 1% β-mercaptoethanol and 0.01% bromophenol blue, and then loaded on 10% Gradi-Gel || gradient gel (Elpis Biotech., Korea). During running, Aβ_{42} peptide distribution was visualized by silver staining. A protein electrophoresis kit was purchased from Bio-Rad Co., USA.

Thioflavin T (ThT) Assay: Incubated Aβ_{42} solutions and dissolved thioflavin T (ThT) solution were mixed into a phosphate buffer (described ahead in 2.4), to a final concentration of 4 vol.% Aβ_{42} solutions and 20×10^{-6} M of ThT solution in a buffer. Then the fluorescence of ThT was analyzed by spectrofluorophotometer (Shimadzu Inc., Japan) to get the emission peak at around 485 nm.

Circular dichroism (CD) Analysis: Far-UV (190-260 nm) CD spectra were measured by a spectropolarimeter (Jasco Inc., Japan) at 20 °C. Conformational changes of peptides were analyzed at 195 and 215 nm. Samples were measured three times under N_2 blowing atmosphere.

Detection of Singlet Oxygen Generation: 100×10^{-6} M of singlet oxygen sensor green (SOSG, Life technologies., USA) was mixed with each solution (none, g-C_3N_4 or metal ion doped g-C_3N_4 in a phosphate buffer), to 1 vol.% of a final concentration. Under light or without light condition, fluorescence of solutions was measured every 20 min by spectrofluorophotometer (Shimadzu Inc., Japan) to obtain SOSG emission peak at 525 nm.

DNPH Assay: The DNPH assay was performed according to the literature.[31] Briefly, 480 µL of each 40×10^{-6} M Aβ_{42} solution was precipitated with a trichloroacetic acid (TCA, 20% final concentration) solution for 10 min in an ice bath and then collected as a form of pellet in a tube by centrifuging (4 min at 14 000 rpm). After that, 500 µL of 10×10^{-3} M DNPH in 2 M of HCl was added into each tube for 1 h at room temperature. Each sample was precipitated with 20% TCA solution and remains were washed three times with 1 mL of ethanol-ethyl acetate (1:1, v/v) solution. Washed samples were resuspended in a guanidine hydrochloride solution (6 M, pH 2.3) for 15 min at 37 °C. Then, the samples were measured by spectrophotometer (Jasco Inc., Japan) to get UV–vis absorbance spectrum (300–600 nm).

MTT Assay: Rat pheochromocytoma-derived PC12 cells (KTCT, Korea) were cultured in RPMI 1640 media with 10% HS, 5% FBS, and 1% antibiotics. Incubation condition was 5% CO_2 atmosphere at 37 °C and cells were sub-cultured at least twice a week. 10×10^4 cells mL^{-1} were seeded into 96 well plates and incubated for 24 h to be attached to the bottom of the wells. 4 µL of preformed Aβ_{42} aggregates, which were incubated under each condition (Aβ_{42} monomers only under dark or light, Aβ_{42} monomers with 100 µg mL^{-1} of g-C_3N_4 or Fe-doped g-C_3N_4 under dark or light), were added and coincubated for an additional 12 h. Cell viability depending on pristine g-C_3N_4 or metal@CN concentration was observed similarly without adding Aβ_{42} aggregates. After that, the medium was eliminated and replaced with a fresh medium containing 10% MTT solution (5 mg mL^{-1} of MTT powder in a phosphate buffer saline). The resulting formazan (purple colored product) absorbance was measured at 595 nm using a Victor 3 microplate reader (PerkinElmer Inc., USA).

Statistical Analysis: Statistical evaluation was performed by means of one-way analysis of variance (ANOVA). Data shown in the figure were means of triplicates with standard deviation (mean ± SD).

Supporting Information

Supporting Information is available from the Wiley Online Library or from the author.

Acknowledgements

This study was supported by the National Research Foundation via the Creative Research Initiative Center (Grant No. NRF-2015R1A3A2066191), South Korea.

Received: November 30, 2015
Revised: March 2, 2016
Published online: April 25, 2016

[1] A. Alzheimer's, *Alzheimer's Dementia* **2014**, *10*, e47.
[2] D. M. Walsh, D. J. Selkoe, *J. Neurochem.* **2007**, *101*, 1172.
[3] I. Benilova, E. Karran, B. De Strooper, *Nat. Neurosci.* **2012**, *15*, 349.
[4] J. Bieschke, M. Herbst, T. Wiglenda, R. P. Friedrich, A. Boeddrich, F. Schiele, D. Kleckers, J. M. Lopez del Amo, B. A. Grüning, Q. Wang, M. R. Schmidt, R. Lurz, R. Anwyl, S. Schnoegl, M. Fändrich, R. F. Frank, B. Reif, S. Günther, D. M. Walsh, E. E. Wanker, *Nat. Chem. Biol.* **2012**, *8*, 93.
[5] Q. Chen, C. Wang, L. Cheng, W. He, Z. Cheng, Z. Liu, *Biomaterials* **2014**, *35*, 2915.
[6] S. S. Lucky, K. C. Soo, Y. Zhang, *Chem. Rev.* **2015**, *115*, 1990.
[7] A. Hirabayashi, Y. Shindo, K. Oka, D. Takahashi, K. Toshima, *Chem. Commun.* **2014**, *50*, 9543.
[8] B. I. Lee, S. Lee, Y. S. Suh, J. S. Lee, A.-k. Kim, O. Y. Kwon, K. Yu, C. B. Park, *Angew. Chem. Int. Ed.* **2015**, *54*, 11472.
[9] J. S. Lee, B. I. Lee, C. B. Park, *Biomaterials* **2015**, *38*, 43.
[10] T. Lin, L. Zhong, J. Wang, L. Guo, H. Wu, Q. Guo, F. Fu, G. Chen, *Biosens. Bioelectron.* **2014**, *59*, 89.
[11] X. Zhang, X. Xie, H. Wang, J. Zhang, B. Pan, Y. Xie, *J. Am. Chem. Soc.* **2013**, *135*, 18.
[12] J. Wang, R. Liu, C. Zhang, G. Han, J. Zhao, B. Liu, C. Jiang, Z. Zhang, *RSC Adv.* **2015**, *5*, 86803.
[13] R. Chen, J. Zhang, Y. Wang, X. Chen, J. A. Zapien, C.-S. Lee, *Nanoscale* **2015**, *7*, 17299.
[14] X.-L. Zhang, C. Zheng, S.-S. Guo, J. Li, H.-H. Yang, G. Chen, *Anal. Chem.* **2014**, *86*, 3426.
[15] Y. Wang, X. Wang, M. Antonietti, *Angew. Chem. Int. Ed.* **2012**, *51*, 68.
[16] Y. Zhang, Q. Pan, G. Chai, M. Liang, G. Dong, Q. Zhang, J. Qiu, *Sci. Rep.* **2013**, *3*.
[17] Z. Ding, X. Chen, M. Antonietti, X. Wang, *ChemSusChem* **2011**, *4*, 274.
[18] X. Lu, K. Xu, P. Chen, K. Jia, S. Liu, C. Wu, *J. Mater. Chem. A* **2014**, *2*, 18924.
[19] S. Yang, Y. Gong, J. Zhang, L. Zhan, L. Ma, Z. Fang, R. Vajtai, X. Wang, P. M. Ajayan, *Adv. Mater.* **2013**, *25*, 2452.
[20] C. Barrow, M. Zagorski, *Science* **1991**, *253*, 179.
[21] H. Levine, *Protein Sci.* **1993**, *2*, 404.
[22] S. C. Yan, Z. S. Li, Z. G. Zou, *Langmuir* **2010**, *26*, 3894.
[23] Y. Gong, M. Li, H. Li, Y. Wang, *Green Chem.* **2015**, *17*, 715.
[24] Y. Tang, Y. Su, N. Yang, L. Zhang, Y. Lv, *Anal. Chem.* **2014**, *86*, 4528.
[25] Y. Li, W. Zhang, J. Niu, Y. Chen, *ACS Nano* **2012**, *6*, 5164.
[26] R. L. Levine, D. Garland, C. N. Oliver, A. Amici, I. Climent, A.-G. Lenz, B.-W. Ahn, S. Shaltiel, E. R. Stadtman, *Methods Enzymol.* **1990**, *186*, 464.
[27] X. Wang, X. Chen, A. Thomas, X. Fu, M. Antonietti, *Adv. Mater.* **2009**, *21*, 1609.
[28] S. Cao, J. Low, J. Yu, M. Jaroniec, *Adv. Mater.* **2015**, *27*, 2150.
[29] S. Zhang, J. Li, M. Zeng, J. Li, J. Xu, X. Wang, *Chem. Eur. J.* **2014**, *20*, 9805.
[30] J. Geng, M. Li, J. Ren, E. Wang, X. Qu, *Angew. Chem. Int. Ed.* **2011**, *50*, 4184.
[31] I. Dalle-Donne, R. Rossi, D. Giustarini, A. Milzani, R. Colombo, *Clin. Chim. Acta* **2003**, *329*, 23.

